https://doi.org/10.20965/jrm.2020.p0984

Paper:

Development of Hydraulic Pump Drive System Using Switched Reluctance Motor with Servo Function

Ha Tham Phan*, **Seiya Itagaki***, **and Yasukazu Sato****

*Department of Mechanical Engineering, Graduate School of Engineering, Yokohama National University
79-5 Tokiwadai, Hodogaya-ku, Yokohama, Kanagawa 240-8501, Japan
E-mail: {ha-phan-dz, itagaki-seiya-kx}@ynu.ac.jp
**Department of Mechanical Engineering, Faculty of Engineering, Yokohama National University
79-5 Tokiwadai, Hodogaya-ku, Yokohama, Kanagawa 240-8501, Japan
E-mail: sato-yasukazu-zm@ynu.ac.jp

[Received March 31, 2020; accepted July 30, 2020]

A switched reluctance motor (SRM) generates a reluctance torque without the power of a permanent magnet, rendering it a candidate for rare-earth free motors. Compared with a permanent magnet synchronous motor (PMSM), SRMs also offer operational advantage in high-temperature environments owing to their robust structure. However, SRMs are generally inferior to PMSMs in terms of torque ripple, noise, and speed control, in particular. Therefore, this study attempts to improve the controllability of SRMs by proposing an SRM driving method in the form of a bidirectional rotation torque and a speed-controllable servomotor. The advantage of this method is evaluated experimentally using a closed-loop hydraulic system (valveless control system), which includes a hydraulic pump driven by an SRM to supply hydraulic power to actuators. The results show that the pump flow rate and hydraulic motor speed are consistent with the sinusoidal commands corresponding to the forward and reverse rotations of the SRM.

Keywords: hydraulic pump, actuator, switched reluctance motor, servomotor, closed hydraulic circuit

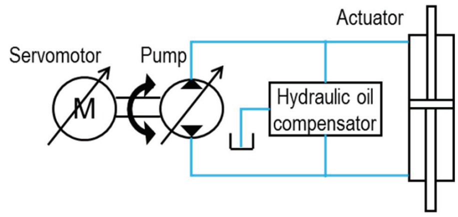

Fig. 1. Valveless control system for hydraulic actuator drive (closed circuit).

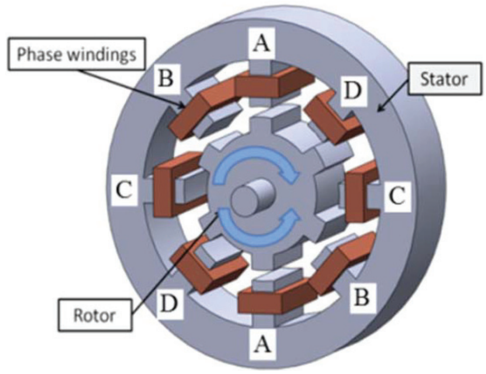

Fig. 2. Typical structure of 8/6-type SRM.

1. Introduction

To improve the power-transmission efficiency in fluid power systems, flow rate control by the rotational speed control of hydraulic pumps not using any control valves is an efficient solution. By removing control valves, which provide flow resistance and generate leakages, a valveless control system utilizing a hydraulic pump driven by a high-performance electric servomotor can be realized to provide a high power-transmission efficiency without pressure drop and leakage power loss, as shown in **Fig. 1**.

In industrial applications, a permanent magnet synchronous motor (PMSM) is used as a high-performance electric servomotor to drive a hydraulic pump in a closed hydraulic circuit. However, PMSMs are expensive and present a few drawbacks due to permanent magnets, such as insufficient heat and vibration resistance and a significant usage of rare-earth materials. Hence, a servomotor function is integrated into a conventional switched reluctance motor (SRM) control. The SRM shown in **Fig. 2** is robust and requires no permanent magnet and rare-earth materials owing to its driving principle. Compared with permanent magnet and induction motors, SRMs have a simpler and more robust construction owing to its rotor structure without coils or permanent magnets, thereby affording a lower fabrication cost. Moreover, SRMs can provide similar or higher efficiencies in the medium and high-speed ranges. SRMs can deliver comparable or superior efficiencies over the entire operation or drive cycle of the application. Another advantage of the SRM is its fault-tolerant operation as each phase of the SRM can be considered as electrically isolated from each other.

Generally, an SRM is used in drive systems requiring high torque outputs in a wide speed range, one-directional rotation, and approximate speed control. To utilize SRMs for driving hydraulic pumps in closed hydraulic circuits, the controllability of the SRM must be improved, such as its bidirectional startup and a wide range of speed regulations. Yamai et al. [1] optimized the SRM motor drive parameters of a hydraulic pump unit using an open hydraulic circuit. They improved the motor efficiency by 6%, reduced the power consumption by 50%, and reduced the acoustic noise level by 5 dBA. Hamdy et al. [2] proposed a starting technique that exploits the natural magnetic asymmetry in the symmetrical machine geometry to provide bidirectional torque production at startup. However, this technique could not regulate the speed of the motor and was applied for only a 4/2 SRM with a low starting torque requirement. Gu et al. [3] focused on a phase shift design strategy to ensure both a large starting torque and bidirectional startup capability for a two-phase switched reluctance machine; however, the speed control function was not mentioned in the study. The studies mentioned above are related to bidirectional rotation SRM control. Other studies related to SRM control, such as [4–9], did not mention such a topic. Meanwhile, several studies have reported hydraulic closed circuits that use power sources other than SRMs, such as permanent magnet synchronous servomotors and induction motors [10–18]. However, the concept of driving a bidirectional rotation-type hydraulic pump using an SRM has not been reported. Herein, a driving method for SRMs is proposed in the form of a bidirectional rotation torque and a speed-controllable servomotor. Furthermore, the performance is evaluated based on the flow rate control of the hydraulic pump driven by the switched reluctance (SR) servomotor in a closed hydraulic circuit.

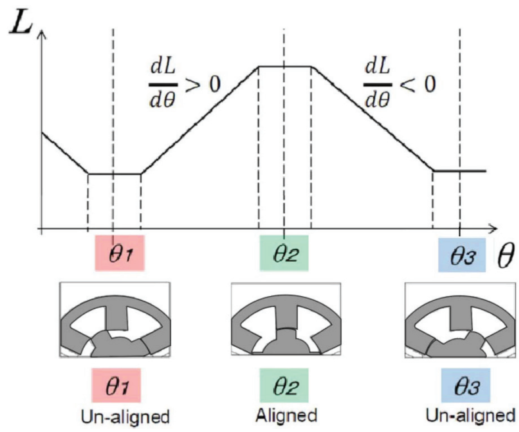

Fig. 3. Inductance change in rotational direction of rotor, L: flux linkage; θ: rotor angular position.

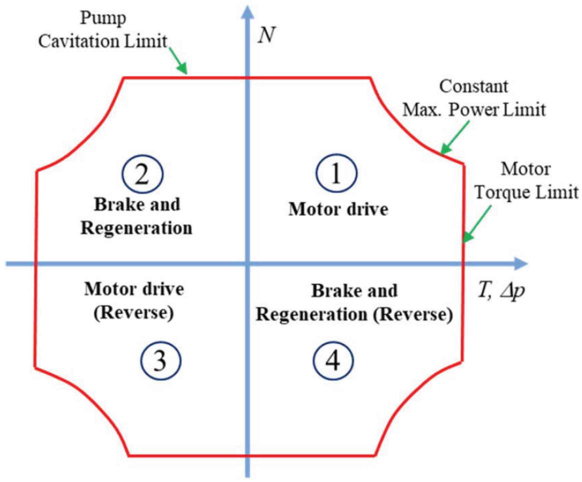

Fig. 4. Four-quadrant operation of hydraulic pump driven by servomotor, T: motor torque; Δp: pressure difference at the pump; N: speed of motor/pump.

2. Operational Principle of SRM

An SRM is identified by the numbers of stator and rotor poles. A typical SRM has salient poles on both the stator and rotor, and its windings are wound only on the stator, as shown in **Fig. 2**.

The sets of opposing poles of the stator are denoted as phases A, B, C, and D. Stator windings that generate a magnetic flux penetrating the air gap between the rotor and stator are wound in series in each phase, and four phases are connected in parallel. In this study, an 8/6-type structure with four phases, a 6-teeth rotor, and an 8-teeth stator were used. In the SRM, when the winding was excited, a force attracting the salient poles of the rotor and stator was generated, thereby producing a reluctance torque. **Fig. 3** shows the inductance distribution L due to the rotor angular position θ.

As shown in **Fig. 3**, at the unaligned position, the flux linkage is the minimum owing to the large air gap. By contrast, when the rotor and stator poles are aligned, the resulting air gap between the stator and rotor poles is minimized. Here, the flux linkage is at its maximum and is dependent on the excitation current. As a higher level of current is applied, the incremental increase in the flux linkage will decrease owing to the higher magnetic flux density, and hence the saturation level of the core will decrease. **Fig. 4** shows the operating range of a hydraulic pump driven by an SR servomotor. Quadrant ① is the region where the hydraulic power is supplied to the hydraulic actuator by a positive torque with forward rotation; it energizes the phase current in the region of $dL/d\theta$ to be positive, as shown in **Fig. 3**. Quadrant ② is the region where braking is applied to the hydraulic actuator with a negative torque and a forward rotation. At the time of transition to the region of negative $dL/d\theta$ shown in **Fig. 3**, the magnetic flux remains and is disconnected from the power supply, and a negative torque is generated by power regeneration. When the negative torque is insufficient, the power supply is connected and the phase current is energized to increase the negative torque. Quadrants ③ and ④ are the states in the reverse rotational directions of ① and ② respectively.

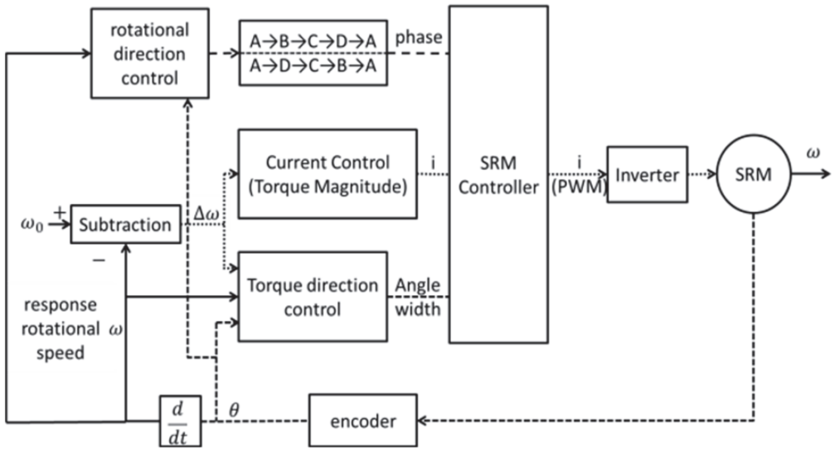

Fig. 5. Bidirection rotational speed control system of SRM.

3. Control Principle of SRM

To operate the four-quadrant drive in the N-T coordinated plane shown in **Fig. 4**, the control method for the SR servomotor should possess the following controls [19, 20].

1) Firing order control (rotational direction control)

The rotational direction is decided by the order of phase excitations. In other words, the SRM rotates in the forward direction by firing order A-B-C-D-A and in the reverse direction by firing order A-D-C-B-A, as shown in **Fig. 2**.

2) Torque amplitude control

The SRM has a salient structure, which is essential for its torque production mechanism. Therefore, the characteristics of the SRM, such as flux linkage and torque, are functions of the rotor position. Furthermore, these characteristics depend on the phase current.

The torque amplitude of an SRM is expressed as shown in Eq. (1) [6].

$$T = \frac{1}{2} i^2 \frac{dL}{d\theta}, \quad \ldots\ldots\ldots\ldots\ldots \quad (1)$$

where T, i, L, and θ are the output torque of the SRM, electric current of the winding, inductance, and rotor teeth angular position of the SRM, respectively. The amplitude of the output torque is controlled by the current of the winding in each phase. The magnitude of the phase current is controlled by pulse width modulation (PWM) switching under a constant voltage supply.

3) Torque direction control

The torque direction is determined by the position of the rotor teeth during firing. The region of positive $dL/d\theta$ – the range where L in **Fig. 3** increases upward to the right, is known as the motor region. When firing in this region, a positive torque is generated, and the SRM accelerates. The region of negative $dL/d\theta$ – the range where L in **Fig. 3** decreases downward to the right is known as the generator region, where a negative torque is also generated in the same manner in the region, and the SRM decelerates. Furthermore, if the magnetic flux remains at the time of transition to this region, an electromotive force yielding a magnetic field that hinders a decrease in the magnetic flux owing to a decrease in inductance is generated in the winding, and a power generation/regeneration that continues to flow a phase current without connection to the power supply is performed.

The angular position of the rotor was detected using a rotary encoder. The controller of the SRM determines the appropriate angle and angle range for generating a positive or negative torque based on the command. As shown in **Fig. 2**, the datum of the angle of the rotor position was set to 0° as the rotor and stator poles were aligned. Based on previous studies [19, 20], when exciting on the plus side in the motor region and the excitation range is from $-30°$ to $-15°$, current begins to be applied to the generator region and rotation is prevented. Therefore, the excitation range was set to $-30°$ to $-15°$. In the generator region, as the braking force was the largest, the excitation range was set from 0° to 15°.

4. Proposed SRM Controller

Figures 5 and **6** show a schematic diagram of the SRM controller. The magnitude of the phase current is determined by the PI control according to the difference in the response speed between the SRM and the command speed. The direction of the torque is determined by the sign of the value (positive or negative) denoting the difference between the command and response speeds, or between the positive and negative response speeds. Moreover, it is determined by the command rotational direction and the response speed direction in the servo-drive control. As shown in **Fig. 6**, the control signal for switching devices such as field effect transistors was sent from the DSP installed in the driving program of the SRM.

In this study, a special control model was added in the startup drive because an incremental rotary encoder was used. To determine the appropriate excitation timing to

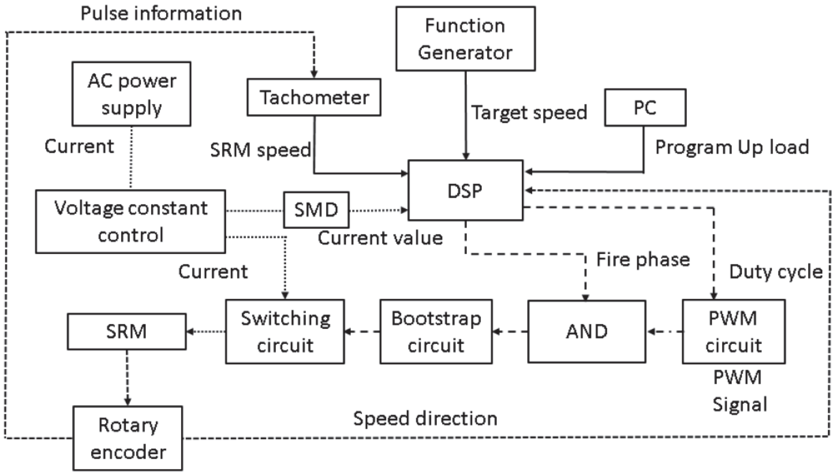

Fig. 6. System flow of SRM drive system.

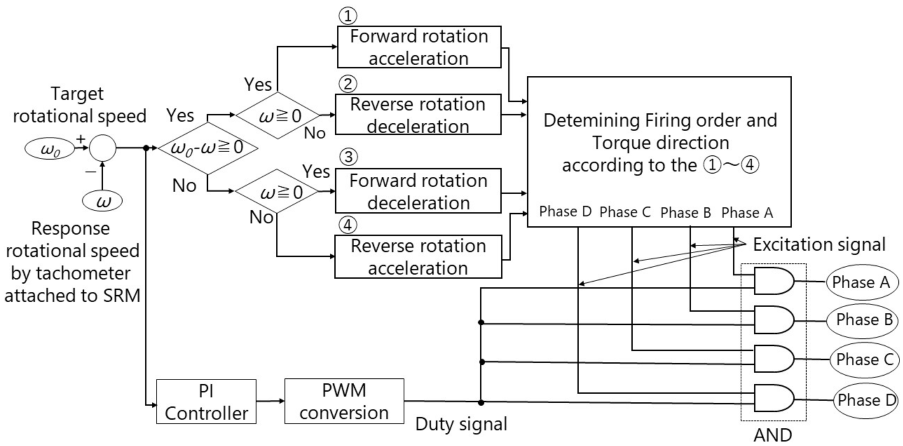

Fig. 7. SRM drive system.

drive the SRM, it is necessary to accurately determine the origin of the SRM body (origin of the rotor) in the startup drive. It is desirable to calculate the angle origin of the SRM body as the position of the A-phase allied position (the part where the inductance has the maximum value). When the SRM was started, to calculate using this position as the origin, t_{step} (0.5 s) was excited in the order of A-phase→B-phase→C-phase→D-phase→A-phase, and the A-phase was forced to be the allied position. This “startup” procedure is then followed by the driving of the SRM, as shown in **Fig. 7**.

In the SRM drive system after the “startup” processing, the rotation was stopped, and information regarding the rotor angle origin (rotary encoder reset origin) was acquired. When starting the SRM, whether the rotation was a forward or reverse rotation was determined based on the drive command signal, and the order was A-phase→B-phase→C-phase→D-phase→A-phase (positive direction). The combination of the rotor angle and excitation phase was set such that the excitation of each phase proceeded in the excitation order in which the rotation continued.

In the reverse rotation, a combination of the rotor angle and excitation phase was set in the order of A-phase→D-phase→C-phase→B-phase→A-phase (the excitation order in which the reverse rotation continued). The torque of the forward/reverse rotation was determined based on the magnitude of the phase winding current, regardless of the rotation direction. Therefore, the winding current was PWM-controlled to be consistent with the target rotation speed.

Furthermore, in the motoring/regeneration state, the section where the winding current of the phase was conducted indicated a positive gradient ($dL/d\theta > 0$, motoring) or a negative gradient ($dL/d\theta < 0$) of the inductance distribution of the SRM. Therefore, to control the SRM like a servomotor with both forward and reverse rotations, variable torques, and switching between motoring and regenerative modes, regeneration must be performed by motoring or rotating based on the excitation phase order according to the rotating direction, winding current magnitude, and rotor angle. Furthermore, control must be performed continuously by combining the three elements of winding energization timing in the region.

Table 1. Experimental condition.

	Motor mode	Generator mode
Command speed	0 to +1000 (rpm)	−1000 to 0 (rpm)
Command waveform	Step response, frequency response	

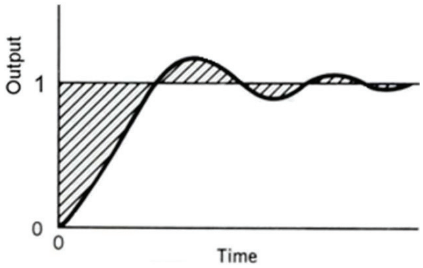

Fig. 8. Illustration of square error area.

5. PI gain Design for Improving Drive System Program

5.1. Purpose of Experiment

A test was performed to determine the feedback gain of the PI control to determine the control amount of the phase current. The experimental conditions were derived from **Table 1** with reference to the specifications of the hydraulic pump/motor to be directly connected to the SRM.

Typically, cavitation occurs in a hydraulic pump/motor to be used at approximately ±2000 rpm. Therefore, the experimental conditions were determined with a target of 50% rotation speed.

However, the goal of this research was not to obtain the optimum value of the PI gain, but to construct a valve-less hydraulic system using an SR servomotor. Therefore, the differential gain was omitted, and PI control was used. First, the integral gain K_i was determined experimentally. Subsequently, K_i was tuned to 0.1 with proportional gain $K_p = 0$ and a small settling time with a small overshoot and undershoot of the response speed to the target speed of the square wave. Finally, K_p was determined by evaluating the square error area for a series of experimental conditions with different response waveforms.

5.2. Square Error Area

The square error area is one of the indexes used to evaluate the controllability of the target model. The equation is expressed as shown in Eq. (2), and the square error area in the step response is the shaded area shown in **Fig. 8**. In addition, an evaluation criterion to determine whether speed oscillations are allowed near the target speed applies in the square error area.

$$I = \int_0^\infty e^2 dt, \quad (e: \text{ error}) \quad \dots\dots\dots \quad (2)$$

If they are allowed, then the square error area is minimized, but velocity oscillations will occur near the target speed. However, if they are not allowed, then the square error area becomes larger than when they are allowed, but no velocity oscillation occurs. In this case, vibrations are undesirable during the operation of the motor in the electrohydraulic control. Therefore, a criterion that forbids speed vibrations near the target speed was adopted, and the square error area of the response speed to the command speed was obtained.

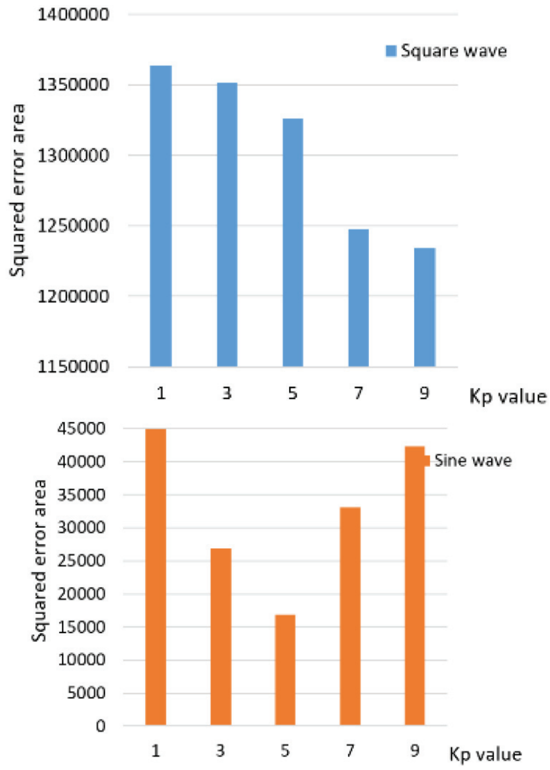

Fig. 9. Squared error area with square wave and sine wave.

5.3. Experimental Results

The values shown in **Figs. 9** and **10** were used to determine the optimal value of the proportional gain. The evaluation method was based on the square error area for one cycle when square and sine waves of 0.5 Hz were the target rotation speed. The amplitude from −1000 to +1000 rpm was considered to be evaluated in both the forward and reverse directions.

The "command voltage" in **Fig. 10** is the deviation of the target speed from the response speed converted into a voltage. This value was input to the power amplifier and then amplified, and the input voltage to the SRM fluctuated. Owing to the specifications of the power amplifier, saturation was applied in the DSP such that the maximum value reached 2.0 V and then plateaued at that value.

The results shown in **Figs. 9** and **10** indicate that the square error area of the step response decreased as the proportional gain increased. This might be because when the command voltage remained longer when it was the upper limit of 2.0 V, the rise was faster. However, even when the proportional gain increased, the rising speed did

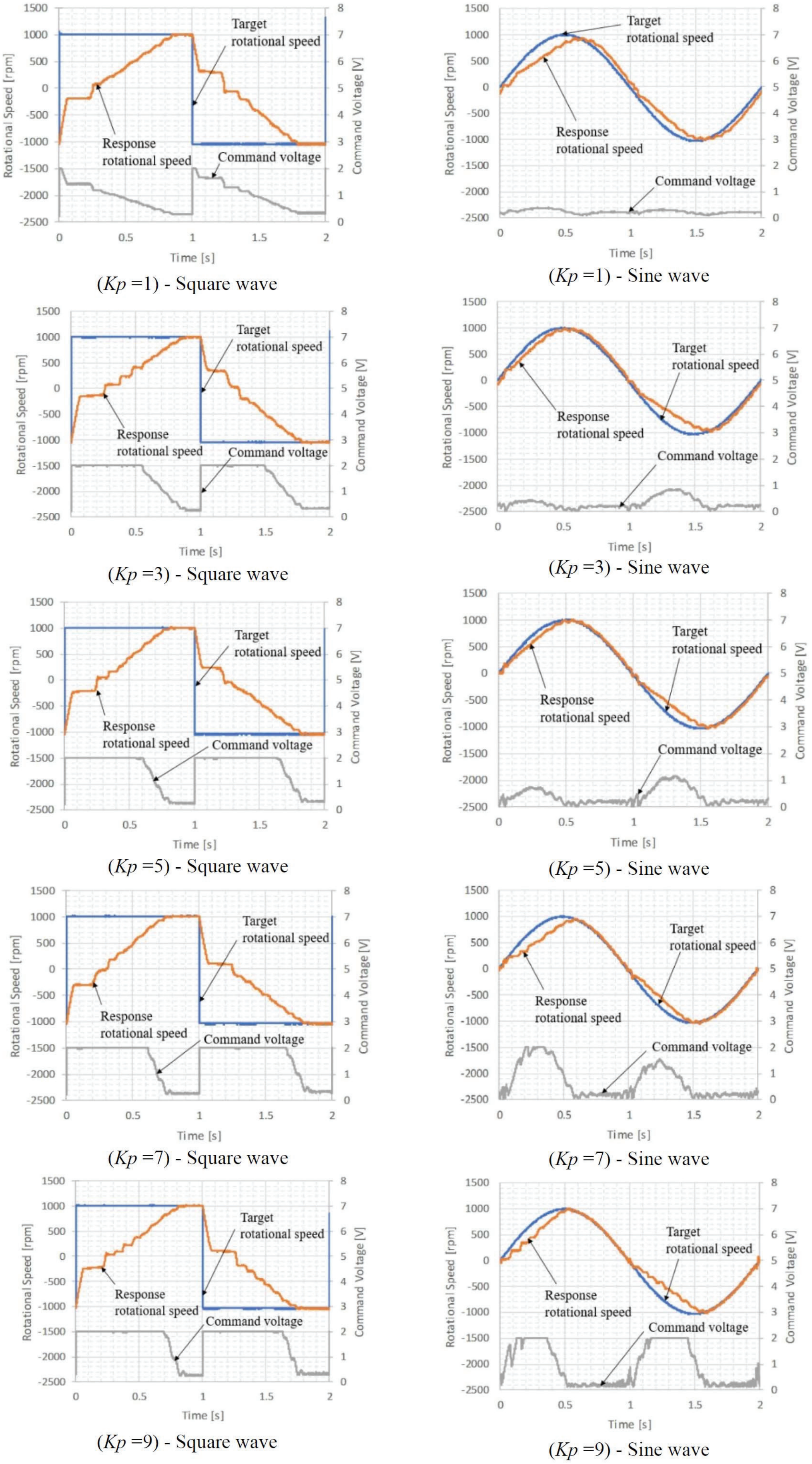

Fig. 10. Experimental results for improving drive system response.

not differ significantly. This is because the output current was limited to 10 A based on the amplifier specifications, and the torque proportional to the square of the current had saturated, as shown in Eq. (1).

As shown in **Figs. 9** and **10** for sine waves, $K_p = 5$ yielded the smallest error. The command voltage reached its maximum when the proportional gain was excessively large. Hence, it was assumed that the allowable current value of the power amplifier had been exceeded, the voltage increased and decreased, the rotation speed oscillated, and the tracking was delayed. In addition, when $K_p = 7$ and $K_p = 9$, near the switching between the normal and reverse rotations of the sine wave in the low-frequency range, oscillations at the following rotational speeds, which were not observed at $K_p = 5$ or less, were observed frequently. Hence, subsequent experiments were performed with $K_p = 5$ and $K_i = 0.1$.

In the subsequent experiments, the response curve to the frequency input of the SRM controlled by the feedback gain derived accordingly is shown in **Fig. 11**. The rotation speed was set to ±500 and ±1000 rpm, and the frequency required in the frequency response was set to 0.5, 1.0, and 2.0 Hz. However, even at 1 Hz, the tracking was delayed for 1000 rpm. When the frequency was 2 Hz, the response curves became almost identical for both 500 and 1000 rpm. These values were considered to be the limits of the switching speed of this circuit. Based on this result, the hydraulic pump/motor drive performed subsequently was controlled with a maximum command waveform of 1000 rpm / 0.5 Hz.

6. Flow Rate Control of Hydraulic Pump Driven by SR Servomotor in Closed-Circuit Applications

Figure 12 shows the applications for the flow rate control of the hydraulic pump driven by the SR servomotor in a closed circuit with an actuator, such as a hydraulic cylinder, hydraulic motor, or rotary cylinder.

Using the proposed SRM controller, the speed and moving/rotating directions of the actuators can be regulated in both directions based on the direction of the SRM.

7. Flow Rate Control Experiment of Hydraulic Pump Driven by SR Servomotor in Closed-Loop Circuit

To evaluate the proposed driving method for the SR motor, a few experimental configurations were implemented for the flow rate control of a fixed displacement bidirectional rotational axial piston pump driven by a four-phase 8/6-type SR servomotor in a closed circuit, as shown in Sections 7.1 and 7.2. **Table 2** shows the specifications of the test SRM and test hydraulic pump/motor.

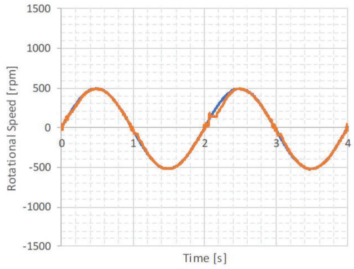

0.5 (Hz) -500 ~ +500 (rpm)

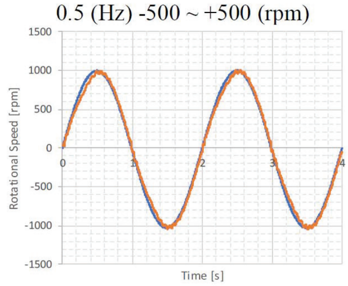

0.5 (Hz) -1000 ~ +1000 (rpm)

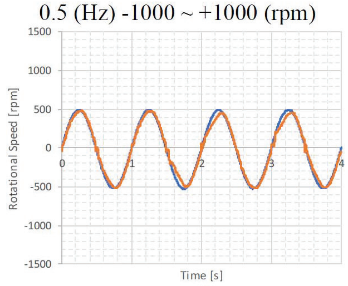

1.0 (Hz) -500 ~ +500 (rpm)

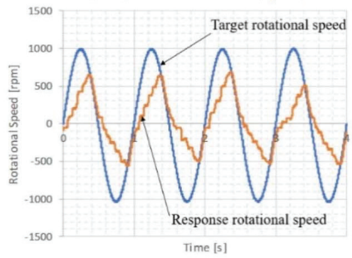

1.0 (Hz) -1000 ~ +1000 (rpm)

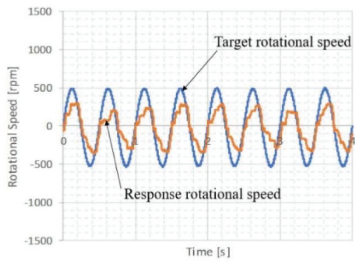

2.0 (Hz) -500 ~ +500 (rpm)

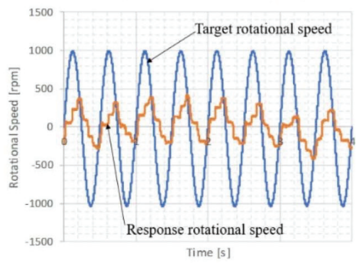

2.0 (Hz) -1000 ~ +1000 (rpm)

Fig. 11. Experimental results for improving drive system response.

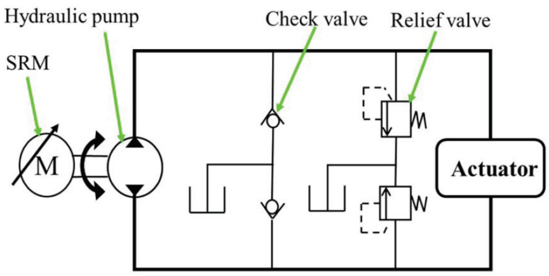

Fig. 12. Hydraulic closed circuit with cylinder and motor application for bidirectional flow rate control using hydraulic servo pump driven by SR servomotor.

Table 2. Specifications of SRM and hydraulic pump/motor.

Switched Reluctance Motor	
Topology	Four-phase 8/6 SRM
Rated Power	490 W
Rated Rotational Speed	8000 rpm
Input Voltage	24 V
Hydraulic Pump/Motor	
Type	Axial piston pump/motor
Displacement	0.8 cm^3/rev
Max. Rotational Speed	2000 rpm (bidirection)
Max. Pressure	16 MPa
Relief Valve	
Set pressure range	5.17~10.3 MPa

7.1. Evaluation of Flow Rate Controllability

As shown in **Fig. 13**, a variable orifice was used as a load in the system. The aim of this experiment was to evaluate the controllability of the pump flow rate and hydraulic oil direction by regulating the SR servomotor. Therefore, the variable orifice was adjusted such that the differential pressure Δp, which is the load, was the value at which the hydraulic pump was driven. Because of the target of this study (as mentioned above), the fluctuation of the differential pressure Δp was not considered in this experiment.

The flow rate of pump Q was estimated from the pump rotation speed N and displacement D_m (Eq. (3)).

$$Q = D_m N \quad (3)$$

Because the maximum rotational speed was 2000 rpm according to the specifications of the test pump, the pump drive was set to rotate bidirectionally with amplitudes of $\pm$1000 rpm / 0.5 Hz and $\pm$500 rpm / 0.5 Hz to ensure the self-suction performance of the pump and to prevent cavitation.

As shown in **Fig. 14**, the pump flow rate was consistent with the sinusoidal command corresponding to the forward and reverse rotations of the SRM. Hence, it was confirmed that the flow direction was switched smoothly even in the vicinity where the rotational direction of the SRM was switched and the flow rate was 0.

7.2. Evaluation of Hydraulic Motor Speed Response

In the subsequent experiment, a fixed displacement bidirectional rotation axial piston motor was installed into

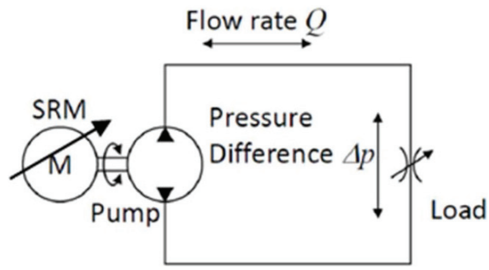

Fig. 13. Bidirectional rotational speed control system of SRM with variable orifice load.

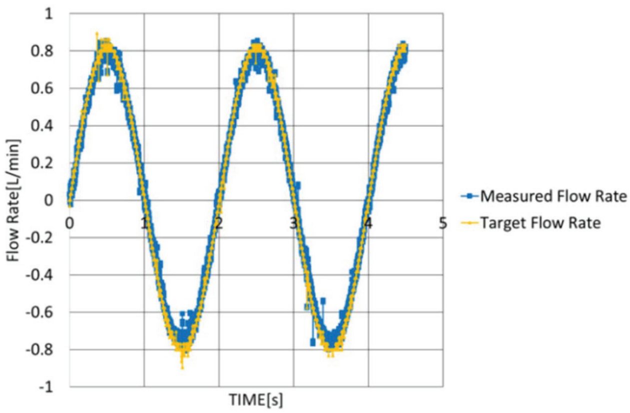

Fig. 14. Sinusoidal bidirection flow rate control of hydraulic pump driven by SR servomotor (SRM speed -1000 to $+1000$ rpm, sine wave 0.5 Hz).

the system, as shown in **Fig. 15**. Because the rated rotational speed of the SRM was significantly higher than the maximum rotational speed of the hydraulic pump, a planetary gear reducer (with a gear ratio of five) was used to connect the SR motor and hydraulic pump to increase the applied torque to the hydraulic pump. The aim of the experiment shown in **Fig. 15** was to evaluate the speed response of the hydraulic motor compared with the command and SRM speed response. **Fig. 16** shows the experimental results of the speed and flow rate control of the hydraulic pump driven by the SR servomotor. The target flow rate was converted to the command signal of the SR motor, and the measured flow rate was obtained using Eq. (3).

As shown in **Fig. 16**, the hydraulic motor speed was consistent with the sinusoidal command corresponding to the forward and reverse rotations of the SRM. However, the SRM speed and hydraulic motor speed deviated slightly at the maximum speed points shown in **Fig. 16**. This may be explained by the volumetric losses in the hydraulic pump and hydraulic motor.

In this experimental setup, the load was the only variable orifice in the hydraulic closed circuit. This system can be applied to a load as a hydraulic cylinder, enabling the moving direction, position, and speed of the cylinder to be controlled.

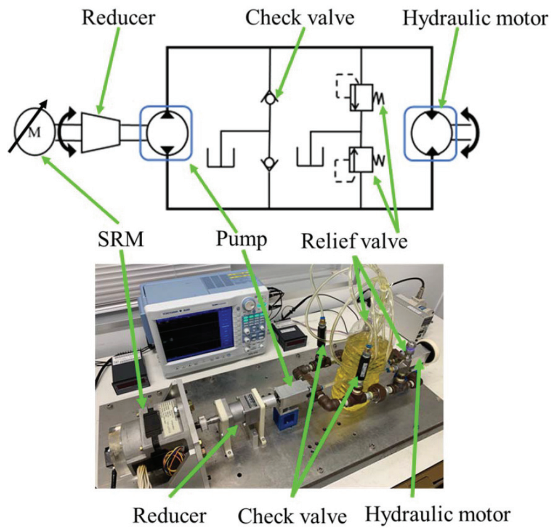

Fig. 15. Bidirectional rotational speed control system of SRM with hydraulic motor.

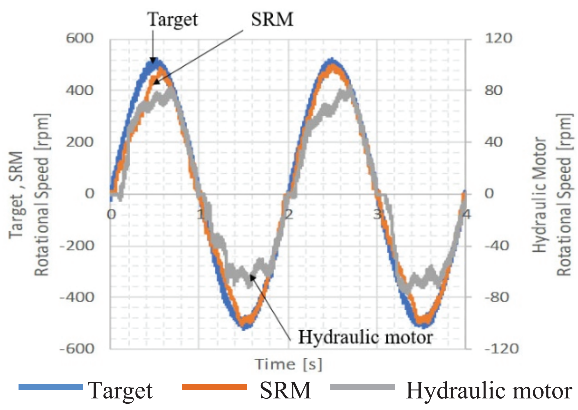

Fig. 16. Sinusoidal bidirection speed control of hydraulic pump driven by SR servomotor (SRM speed −500 to +500 rpm, sine wave 0.5 Hz).

8. Conclusion

A control system for an SR motor with a servo function added to the SRM was proposed herein. Subsequently, the closed-circuit flow control performance of a pump driven by an SR servomotor was presented. This method solved problems arising from the permanent magnets of the motor in the flow rate control system of a hydraulic closed-loop circuit. The experimental results confirmed that the flow rate direction was switched smoothly even in the vicinity where the rotational direction of the SRM was switched and the flow rate was 0. The authors will consider the effects of the speed-torque characteristics of the system by conducting further experiments that include inertial loads.

References:

[1] H. Yamai, M. Kaneda, K. Ohyama,Y. Takeda, and N. Matsui, "Optimal Switched Reluctance Motor Drive for Hydraulic Pump Unit," IEEE Conf. on Industry Applications, Vol.3, pp. 1555-1562, doi:10.1109/IAS.2000.882089, 2000.

[2] R. Hamdy, J. Fletcher, and B. W. Williams, "Bidirectional Starting of a Symmetrical Two-Phase Switched Reluctance Machine," IEEE Trans. on Energy Conversion, Vol.15, No.2, pp. 211-217, doi:10.1109/60.867002, 2000.

[3] L. Gu, W. Wang, B. Fahimi, A. Clark, and J. Hearron, "Magnetic Design of Two-Phase Switched Reluctance Motor With Bidirectional Startup Capability," IEEE Trans. on Industry Applications, Vol.52, No.3, pp. 2148-2155, doi:10.1109/TIA.2016.2514356, 2016.

[4] S. Wei, S. Zhao, and J. Zheng, "Self-Tuning Fuzzy Control of Switched Reluctance Motor Directly-driven Hydraulic Press," WRI World Congress on Software Engineering, Xiamen, pp. 461-465. doi:10.1109/WCSE.2009.164, 2009.

[5] J. Ahn and G. F. Lukman, "Switched reluctance motor: Research trends and overview," CES Trans. on Electrical Machines and Systems, Vol.2, No.4, pp. 339-347, doi:10.30941/CESTEMS.2018.00043, 2018.

[6] T. J. E. Miller, "Switched Reluctance Motors and Their Control," Clarendon Press, 1993.

[7] B. Bilgin, J. W. Jiang, and A. Emadi, "Switched Reluctance Motor Drives – Fundamentals to Applications," CRC Press, doi:10.1201/9780203729991, 2019.

[8] T. Husain, W. Uddin, and Y. Sozer, "Performance Comparison of Short Pitched and Fully Pitched Switched Reluctance Machines Over Wide Speed Operations," IEEE Energy Conversion Congress and Exposition (ECCE), doi:10.1109/TIA.2018.2839627, 2016.

[9] K. Aiso and K. Akatsu, "High Speed SRM using vector Control for Electric Vehicle," CES Trans. on Electrical Machines and Systems, Vol.4, No.1, pp. 61-68, doi:10.30941/CESTEMS.2020.00009, 2020.

[10] H. Tanaka, H. Kaminaga, and Y. Nakamura, "Pressure feedback control based on singular perturbation method of an electro-hydrostatic actuator for an exoskeletal power-assist system," J. Robot. Mechatron., Vol.24, No.2, pp. 354-362, 2012.

[11] H. Zhang, X. Liu, J. Wang, and H. E. Karimi, "Robust H_∞Sliding Mode Control with Pole Placement for a Fluid Power Electrohydraulic Actuator (EHA) System," Int. J. of Advanced Manufacturing Technol., Vol.73, No.5, pp. 1095-1104, doi:10.1007/s00170-014-5910-8, 2014.

[12] S. Hyo and S. Tanimoto, "Joint Torque Control of a Hydraulic Manipulator with Hybrid Servo Booster," The 10th Japan Fluid Power System Society (JFPS) Int. Symp. on Fluid Power, 1C11-16, 2017.

[13] K. Rongjie, J. Zongxia, W. Shaoping, and C. Lisha, "Design and Simulation of Electro-hydrostatic Actuator with a Built-in Power Regulator," Chinese J. of Aeronautics, Vol.22, Issue 6, pp. 700-706, doi:10.1016/S1000-9361(08)60161-2, 2009.

[14] Y. Wang, S. Guo, and H. Dong, "Modeling and Control of a Novel Electro-Hydrostatic Actuator with Adaptive Pump Displacement," Chinese J. of Aeronautics, Vol.33, Issue 1, pp. 365-371, doi:10.1016/j.cja.2018.05.020, 2020.

[15] T. Sourander, T. Minav, M. Pietola, and H. Hänninen, "Sensorless Position Control of Direct Driven Hydraulic Actuators," The 10th Japan Fluid Power System Society (JFPS) Int. Symp. on Fluid Power, 2A10, doi:10.5739/jfpsij.11.26, 2017.

[16] A. Navatha, K. Bellad, S. S. Hiremath, and S. Karunanidhi, "Dynamic Analysis of Electro Hydrostatic Actuation System," Global Colloquium in Recent Advancement and Effectual Researches in Engineering, Science and Technology, Vol.25, pp.1289-1296, doi:10.1016/j.protcy.2016.08.223, 2016.

[17] K. Tsuda, K. Umeda, I. Kota, S. Sakaino, and O. Tsuji, "Analysis on Rigidity of Hydraulic Hoses for Electro-Hydrostatic Actuators," 43rd Annual Conf. of the IEEE Industrial Electronics Society, pp. 2828-2833 doi:10.1109/IECON.2017.8216477, 2017.

[18] A. Navatha, S. S. Hiremath, S. Makaram, K. Subramaniam, and A. Talukdar, "Review on Electro Hydrostatic Actuator for Flight Control," Int. J. of Fluid Power, Vol.17, No.2, pp. 125-145, doi:10.1080/14399776.2016.1169743, 2016.

[19] Y. Sato, K. Murakami, and Y. Tsuboi, "Sensorless Torque and Thrust Estimation of a Rotational/Linear Two Degrees-of-Freedom Switched Reluctance Motor," IEEE Trans. Magnetics, Vol.52, No.7, pp. 1-4, doi:10.1109/TMAG.2016.2536682, 2016.

[20] Y. Sato, "Development of a 2-Degree-of-Freedom Rotational/Linear Switched Reluctance Motor," IEEE Trans. Mag, Vol.43, No.6, pp. 2564-2566, doi:10.1109/TMAG.2007.892854, 2007.

Name:
Ha Tham Phan

Affiliation:
Ph.D. Student, Graduate School of Engineering Science, Yokohama National University

Address:
79-5 Tokiwadai, Hodogaya-ku, Yokohama, Kanagawa 240-8501, Japan

Brief Biographical History:
2010 Graduated from Undergraduate School, National University of Civil Engineering
2010- Mechanical Engineer, Science-Technology Institute For Electric-Mechanical Engineering
2011- Lecturer, Department of Construction Machinery, National University of Civil Engineering
2013 Graduated from Graduate School, National University of Civil Engineering
2018- Ph.D. Student, Graduate School of Engineering Science, Yokohama National University

Main Works:
• Saving-energy solutions and control system for hydraulic transmission system

Membership in Academic Societies:
• The Japan Fluid Power System Society (JFPS)

Name:
Yasukazu Sato

Affiliation:
Professor, Faculty of Engineering, Yokohama National University

Address:
79-5 Tokiwadai, Hodogaya-ku, Yokohama, Kanagawa 240-8501, Japan

Brief Biographical History:
1992 Received Doctoral degree from Yokohama National University
1992- Faculty of Engineering, Yokohama National University
2001-2002 Visiting Fellow, University of Glasgow / Visiting Fellow, Royal Institute of Technology Sweden
2012- Professor, Department of Mechanical Engineering, Yokohama National University

Main Works:
• Mechatronics, fluid power system, electromagnetic actuators, and automotive power transmission

Membership in Academic Societies:
• The Japan Society of Mechanical Engineers (JSME)
• The Japan Fluid Power System Society (JFPS)
• Society of Automotive Engineers of Japan (JSAE)
• The Institute of Electrical and Electronics Engineers (IEEE)
• SAE International

Name:
Seiya Itagaki

Affiliation:
Graduate Student, Graduate School of Engineering Science, Yokohama National University

Address:
79-5 Tokiwadai, Hodogaya-ku, Yokohama, Kanagawa 240-8501, Japan

Brief Biographical History:
2019 Graduated from College of Engineering Science, Yokohama National University
2019- Graduate Student, Graduate School of Engineering Science, Yokohama National University

Main Works:
• Electric motor and hydraulic pump in industrial equipment

Membership in Academic Societies:
• The Japan Fluid Power System Society (JFPS)